JACS
JOURNAL OF THE AMERICAN CHEMICAL SOCIETY
Communication
pubs.acs.org/JACS

In Situ Probes of Capture and Decomposition of Chemical Warfare Agent Simulants by Zr-Based Metal Organic Frameworks

Anna M. Plonka,[†] Qi Wang,[†] Wesley O. Gordon,[‡] Alex Balboa,[‡] Diego Troya,[§] Weiwei Guo,[∥] Conor H. Sharp,[§] Sanjaya D. Senanayake,[⊥] John R. Morris,[§] Craig L. Hill,[∥] and Anatoly I. Frenkel*[,†]

[†]Department of Material Science and Chemical Engineering, Stony Brook University, Stony Brook, New York 11794, United States
[‡]U.S. Army Edgewood Chemical Biological Center APG, Aberdeen Proving Ground, Maryland 21010, United States
[§]Department of Chemistry, Virginia Tech, Blacksburg, Virginia 24061, United States
[∥]Department of Chemistry, Emory University, Atlanta, Georgia 30322, United States
[⊥]Department of Chemistry, Brookhaven National Laboratory, Upton, New York 11973, United States

Supporting Information

ABSTRACT: Zr-based metal organic frameworks (MOFs) have been recently shown to be among the fastest catalysts of nerve-agent hydrolysis in solution. We report a detailed study of the adsorption and decomposition of a nerve-agent simulant, dimethyl methylphosphonate (DMMP), on UiO-66, UiO-67, MOF-808, and NU-1000 using synchrotron-based X-ray powder diffraction, X-ray absorption, and infrared spectroscopy, which reveals key aspects of the reaction mechanism. The diffraction measurements indicate that all four MOFs adsorb DMMP (introduced at atmospheric pressures through a flow of helium or air) within the pore space. In addition, the combination of X-ray absorption and infrared spectra suggests direct coordination of DMMP to the Zr_6 cores of all MOFs, which ultimately leads to decomposition to phosphonate products. These experimental probes into the mechanism of adsorption and decomposition of chemical warfare agent simulants on Zr-based MOFs open new opportunities in rational design of new and superior decontamination materials.

Chemical warfare agents (CWAs) continue to present a significant threat in the event of war or terrorist attacks.[1] Current defense technology for filtration and decomposition of CWAs mainly consists of activated carbons in pure or impregnated form. However, significant drawbacks of those filters, such as secondary emission after saturation, low capacity for long-term activation, and ultimate disposal, present an urgent need to develop improved materials capable of fast adsorption and decontamination of CWAs under ambient conditions.[2] These challenges have motivated research into a new generation of sorptive or catalytically active materials for CWA decontamination, including metal oxides,[3,4] polyoxometalates,[5,6] and metal organic frameworks.[7−10]

Metal organic frameworks are a novel class of materials, formed by inorganic cores connected by organic linkers to form extended networks with high porosity and ultrahigh surface areas.[11] MOFs can therefore provide adsorption properties competitive with commercially available adsorbents[12,13] and have found application in gas storage,[13,14] gas separation,[15,16] and catalysis, including catalytic decontamination of toxic chemicals.[17−20] Zr-based MOFs are particularly interesting for catalysis due to their stability in water and at high temperatures.[21−23] Indeed, some Zr-MOFs have been recently proven to decompose CWAs and CWA simulants.[7−10] While these studies have reported turnover frequencies and CWA half-lives on Zr-MOFs, no experimental probes into the atomistic reaction mechanism are available to date.

This Communication provides insight into the atomic-scale mechanism for CWA adsorption and decomposition on four Zr-based MOFs that decompose CWAs and CWA simulants.[9,10,24,25] Specifically, we studied the adsorption of the nerve-agent Sarin simulant DMMP (dimethyl methylphosphonate), on UiO-66 [$Zr_6(\mu_3\text{-}O)_4(\mu_3\text{-}OH)_4(bdc)_6$; bdc: benzene-1,4-dicarboxylate], UiO-67 [$Zr_6(\mu_3\text{-}O)_4(\mu_3\text{-}OH)_4(bpdc)_6$; bpdc: biphenyl-4,4′-dicarboxylate], MOF-808 [$Zr_6(\mu_3\text{-}O)_4(\mu_3\text{-}OH)_4(OH)_6(H_2O)_6(btc)_2$; btc: benzene-1,3,5-tricarboxylate], and NU-1000 [$Zr_6(\mu_3\text{-}O)_4(\mu_3\text{-}OH)_4(OH)_4(H_2O)_4(tbapy)_2$; tbapy: tetratopic 1,3,6,8-tetrakis(*p*-benzoate) pyrene] using in situ synchrotron powder X-ray diffraction (PXRD) and extended X-ray absorption fine-structure spectroscopy (EXAFS). PXRD and EXAFS illuminate both the macroscopic crystalline and atomic length scales, affording a deep understanding of the DMMP−MOF interaction.[26,27] The combination of these two in situ methods is essential for developing an overall understanding of MOF chemistry because they bridge localized site-specific reactions with macroscopic changes in the MOF structures.

All four MOFs studied in this work contain cationic Zr_6 nodes, connected by aromatic carboxylate ligands to form porous frameworks, but the topology of the frameworks differs between them (Figure S1). UiO-66 and UiO-67 are isostructural; in both materials, the nodes are 12-connected with ditopic ligands, resulting in cubic frameworks.[28] The structure of NU-1000 is based on 8-connected Zr_6 nodes and tetratopic tbapy ligands that form a hexagonal network. NU-1000 has significantly larger pores than UiO-66, UiO-67, or MOF-808 with an aperture size of 31 Å.[29] MOF-808 possesses a cubic framework formed by 6-connected Zr_6 nodes and

Received: November 1, 2016
Published: December 30, 2016

ACS Publications © 2016 American Chemical Society

DOI: 10.1021/jacs.6b11373
J. Am. Chem. Soc. 2017, 139, 599−602

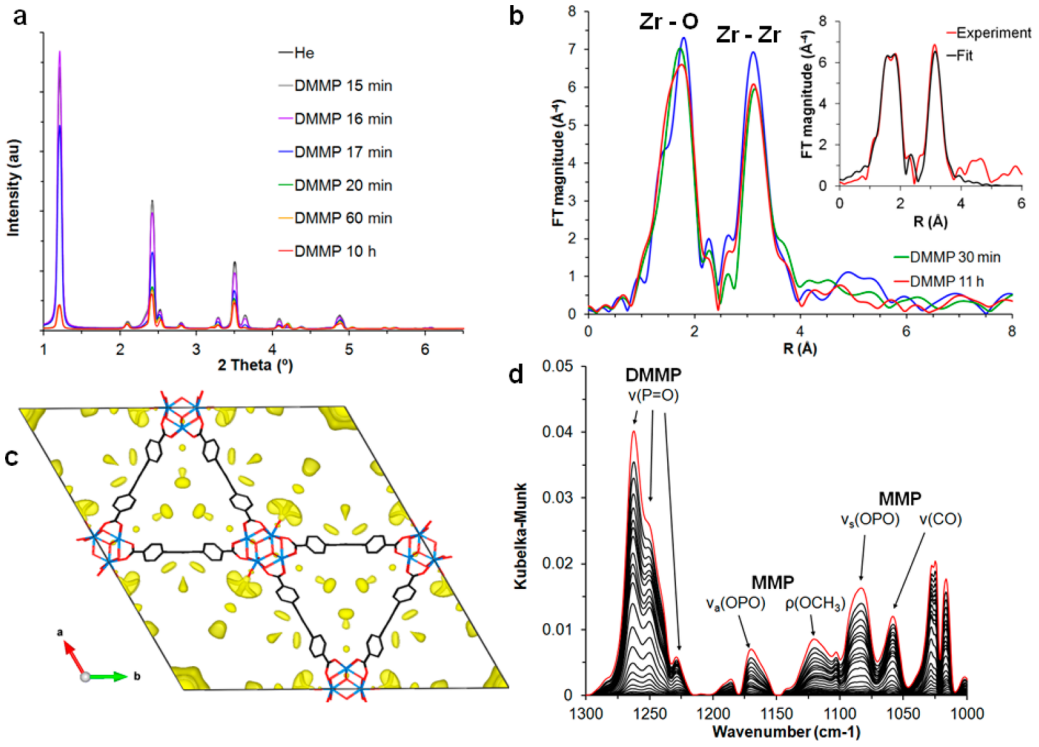

Figure 1. (a) In situ PXRD data of NU-1000 collected during the exposure to DMMP. (b) In situ EXAFS data of NU-1000 collected during the exposure to DMMP. Inset shows experimental and fitted curves for the last DMMP data set. (c) Difference Fourier electron density map of DMMP-treated NU-1000 after 10 h. Zr = blue, C = black, and O = red. Hydrogen atoms have been removed for clarity. Electron density isosurface is drawn at 0.3 $\bar{e}$/Å^3 in yellow. (d) Fingerprint region of time-resolved DRIFTS spectra for DMMP-treated NU-1000. Red line shows the last data set collected after 213 min.

tritopic btc ligands. Because the node is only 6-connected, MOF-808 offers more open Zr sites, and better spatial accessibility than the 12- or 8-connected MOFs.[30]

The stages of DMMP adsorption and reaction on Zr-MOFs were investigated by performing in situ PXRD experiments, where the desolvated samples were exposed to DMMP vapor for up to 11 h. Examination of the collected patterns clearly reveals that each sample undergoes structural changes during exposure. The most apparent change is the decrease in intensity of the low angle reflection relative to higher angle reflections (Figures 1a, S2). This behavior is typically indicative of adsorbents entering porous materials, which suggests that DMMP diffused into the pore space of the MOFs during exposure.[31] A similar, but reverse effect, can be observed upon thermal removal of the adsorbents in a He flow. This thermal desorption process also appears to decompose UiO-66 and UiO-67, as the reflection peaks in Figure S2 significantly broaden and weaken, indicative of framework collapse. Note that, prior to exposure, the MOFs demonstrated thermal stability up to 150 °C; therefore, DMMP or products of DMMP decomposition form strong interactions with the MOFs or produce large capillary forces upon saturation that prevent removal without collapsing the MOF material. In contrast to the UiO MOFs, both MOF-808 and NU-1000 survived removal of the adsorbents. The PXRD patterns of MOF-808 and NU-1000 reveal that He purging and heating did not collapse the materials, but did result in some structural changes (Figure S2).

Apart from changes in the peak intensity, we observed that exposure to DMMP shifts reflections toward lower 2θ angles, indicating the expansion of the lattice for all MOFs (Figures S4–S7). LeBail fits were performed on 10–20 patterns collected during each experiment in order to extract the unit cell parameters. This analysis reveals that, for each MOF, the unit cell expands during the experiment, with the most significant change observed for MOF-808, where the unit cell volume expanded from 44516(6) Å^3 to 45110(6) Å^3 (1.33% increase) after 1 h (Table S1, Figure 2). For UiO-67 and NU-1000, the process starts immediately upon exposure and expansion slows or even reverses slightly following the initial 30 min of exposure (1.17% and 0.76%, respectively). The decreases in UiO-67 volume after 60 min of DMMP dosing suggest either ongoing reaction (provided reaction products have smaller volume than DMMP) or destruction of the material. Finally, the unit cell of UiO-66 changes almost as much as for MOF-808 (1.30%), but the process is much slower, and progresses throughout the 11 h duration of the experiments. The different rates of expansion may be due to the fact that UiO-66 has smaller pores than the other materials and the rate of expansion is limited by slow diffusion.

Beyond structural changes to the MOF, the PXRD data provide insight into the location of adsorbed DMMP and/or products of DMMP decomposition within the MOFs via Fourier difference analysis of the empty and DMMP-loaded frameworks. The starting structural model for the MOF frameworks was refined with the Rietveld method from the data acquired from the desolvated samples in He (Figures S8–S10). The electron density maps calculated for UiO-66, MOF-808, and NU-1000 from the patterns collected at the end of each experiment are shown in the Figure 1c and Figures S11–S12; for UiO-67, the Fourier analysis was not viable (see Supporting Information (SI)). The results indicate that the

DOI: 10.1021/jacs.6b11373
J. Am. Chem. Soc. 2017, 139, 599–602

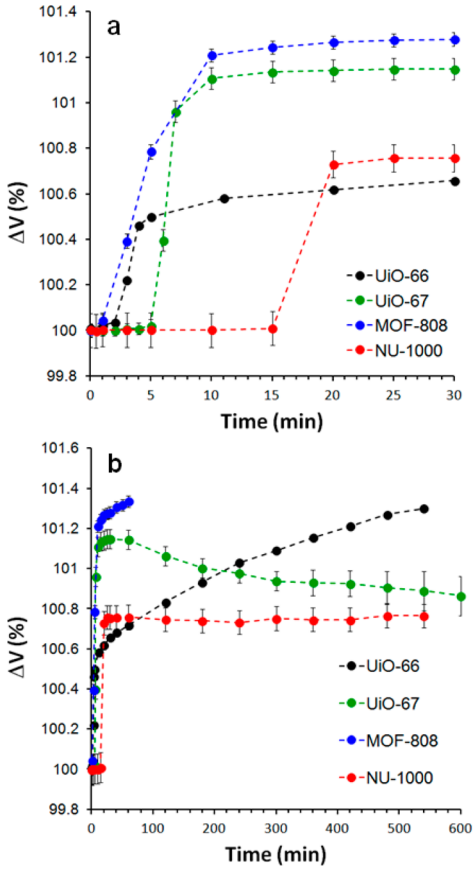

Figure 2. Evolution of UiO-66, UiO-67, MOF-808, and NU-1000 unit cell volumes with the dosing of DMMP (a) first 30 min of dosing and (b) full experiment.

highest electron density increase occurs in the periphery of the Zr_6 clusters, where adsorption/reaction occurs, as well as in the middle of the pores, as expected when the pores become occupied (Figure 1).

To complement the in situ PXRD experiments, we measured the PXRD data from the desolvated samples exposed to DMMP in air ex situ in a closed container for 48 h. Collected data show similar changes to those observed in the in situ experiments, with the peak intensity decreasing and peak position shifting toward lower angles (Figures S13–S16, Table S2). These results suggest that MOFs adsorb DMMP from the air, offering the applicability of these MOFs to real-life conditions.

While the PXRD data revealed key structural changes to the MOFs upon adsorption (and desorption) and that the Zr_6 cluster is the main site for DMMP uptake, additional techniques are required to help determine the reaction mechanism. We performed a series of in situ EXAFS experiments on the Zr K-edge while the MOF samples were exposed to DMMP. For these studies, the desolvated MOFs were exposed to DMMP vapor for up to 11 h with continuous Fourier transform (FT) magnitude data collection. The resulting time-resolved EXAFS plots reveal that, for all samples, the Zr–O and Zr–Zr peaks decrease due to increased disorder (Figures 1b, S17), suggesting that DMMP interacts with Zr directly. Quantitative analysis fully reproduces the previously reported Zr–O and Zr–Zr distances for a hydroxylated UiO-66 MOF (Table S3).[32] The other three MOFs studied here have similar distances between Zr and its nearest O and Zr neighbors, thus confirming that all four MOFs were hydroxylated during the interaction with DMMP. Because the positions of the Zr–Zr peaks did not change during He activation and DMMP exposure, we interpret the reduction in the peak intensity with time as caused by the increased disorder in Zr–O and Zr–Zr distances during adsorption/reaction. The fact that the Zr environment is affected by DMMP exposure, coupled with the results from the diffraction experiments that indicate DMMP enters MOF pores, provides strong evidence that DMMP interacts directly with Zr.

To evaluate the fate of DMMP within the pores of the four MOFs and characterize reaction products, we performed in situ diffuse reflectance Fourier-transform spectroscopy (DRIFTS). In all four cases, spectra show both bands associated with DMMP adsorption and those belonging to the products of decomposition into methyl methylphosphonate (MMP). The main features arising from DMMP adsorption are the peaks assigned as ν(P═O) located between 1200 and 1300 cm^{-1}. The observed MMP modes include ν_a(OPO) at ∼1175 cm^{-1}, ρ(OCH3) at ∼1125 cm^{-1}, ν_s(OPO) at ∼1075 cm^{-1}, and ν(CO) at ∼1060 cm^{-1} (for a detailed description see SI). Although differences in the structural geometry of the MOFs result in varying spectral characteristics, each spectrum produces evidence for DMMP decomposition (Figures S22–S26).

The EXAFS and time-dependent DRIFTS data illuminate the reaction mechanism for the DMMP decomposition on Zr-MOFs. This mechanism is also informed by recent computational work on the decomposition of Sarin on the $Cs_8Nb_6O_{19}$ Lindqvist hexaniobate and Zr-MOFs.[33,34] The starting point of the reaction is a complex in which DMMP is bound to an undercoordinated Zr atom of the MOF adjacent to a Zr–OH group (Scheme 1). The reaction mechanism consists of two

Scheme 1. Mechanism of DMMP Decomposition

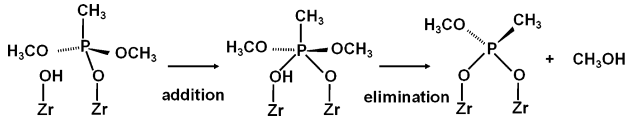

elementary steps: (i) nucleophilic addition of the hydroxide ligand to DMMP to generate a pentacoordinated phosphorus intermediate, and (ii) decomposition of the pentacoordinated intermediate via elimination of methanol (MeOH), to produce methyl methylphosphonate bound to the Zr_6 cores, as suggested by the DRIFTS spectra. As noted in the computational study of Sarin decomposition with Zr-MOFs,[34] elimination of products from the intermediate requires a proton transfer to the leaving group. The proton can be transferred from the hydroxide ligand that undergoes nucleophilic addition, or from a μ_3-OH group in the face of the Zr_6 octahedron. In both cases, the structure of the Zr_6 octahedron is perturbed by the reaction, thus altering the Zr–O and Zr–Zr bonding framework and lowering the intensity of EXAFS oscillations.

Initially, both MeOH and MMPA products are bound to the MOF. MeOH interacts to the MOF via a hydrogen bond, but the MMPA products are strongly bound to the MOF through covalent bonds. In fact, the desorption energy of MMPA (>100 kJ/mol)[34] is large enough that the binding of this phosphonic acid to the MOF is irreversible under ambient conditions.

DOI: 10.1021/jacs.6b11373
J. Am. Chem. Soc. 2017, 139, 599–602

In conclusion, our results show that Zr-MOFs are attractive candidates for future development of CWA decontamination materials at the gas−surface interface. In all four cases, the Sarin simulant DMMP is adsorbed within the pore space, as evident from in situ PXRD data, and undergoes decomposition to MMP species, as evident from DRIFTS results. Further, we showed that DMMP is actively adsorbed from the air, even in the presence of humidity or other ambient gases, demonstrating that Zr_6-based MOFs may serve as effective sorbents for CWAs under ambient conditions. However, our results indicate that exposure of these MOFs to vapor-phase organophosphonates may lead to strongly bound products or MOF collapse that will inhibit the catalytic process that has been extensively reported in solution.[10] Our studies highlight critical design criteria for the development of future vaporous CWA decontamination materials and catalysts. Most importantly, effective materials will require facile diffusion to active sites while avoiding strong binding of phosphonic acid products to the catalyst. In addition, the determination of reaction products reported in this work will stimulate development of postexposure treatments to regenerate the MOF catalysts.

■ ASSOCIATED CONTENT

Supporting Information

The Supporting Information is available free of charge on the ACS Publications website at DOI: 10.1021/jacs.6b11373.

Experimental description, Supplementary Figures S1−S26, and Supplementary Tables S1−S5 (PDF)

■ AUTHOR INFORMATION

Corresponding Author

*anatoly.frenkel@stonybrook.edu

ORCID

Anna M. Plonka: 0000-0003-2606-0477

Diego Troya: 0000-0003-4971-4998

Anatoly I. Frenkel: 0000-0002-5451-1207

Notes

The authors declare no competing financial interest.

■ ACKNOWLEDGMENTS

This work is supported by the U.S. Army Research Laboratory and the U.S. Army Research Office under Grant No. W911NF-15-2-0107. The authors thank the Defense Threat Reduction Agency for support under program BB11PHM156. Use of Advanced Photon Source, Stanford Synchrotron Radiation Lightsource, and National Synchrotron Light Source II was supported by the U.S. Department of Energy under Contract Nos. DE-AC02-06CH11357, DE-AC02-76SF00515, and DE-SC0012704, respectively. In situ operations at the BL2-2 beamline at SLAC were made possible by the U.S. Department of Energy Grant No. DE-SC0012335. A.I.F. and Q.W. thank Prof. C. Lamberti for valuable discussions. The authors are grateful to Prof. J. T. Hupp and Prof. O. K. Farha for generously providing the sample of NU-1000.

■ REFERENCES

(1) Yang, Y. C.; Baker, J. A.; Ward, J. R. *Chem. Rev.* **1992**, *92*, 1729.

(2) Smith, B. M. *Chem. Soc. Rev.* **2008**, *37*, 470.

(3) Wagner, G. W.; Peterson, G. W.; Mahle, J. J. *Ind. Eng. Chem. Res.* **2012**, *51*, 3598.

(4) Bandosz, T. J.; Laskoski, M.; Mahle, J.; Mogilevsky, G.; Peterson, G. W.; Rossin, J. A.; Wagner, G. W. *J. Phys. Chem. C* **2012**, *116*, 11606.

(5) Kinnan, M. K.; Creasy, W. R.; Fullmer, L. B.; Schreuder-Gibson, H. L.; Nyman, M. *Eur. J. Inorg. Chem.* **2014**, *2014*, 2361.

(6) Guo, W.; Lv, H.; Sullivan, K. P.; Gordon, W. O.; Balboa, A.; Wagner, G. W.; Musaev, D. G.; Bacsa, J.; Hill, C. L. *Angew. Chem., Int. Ed.* **2016**, *55*, 7403−7407.

(7) López-Maya, E.; Montoro, C.; Rodríguez-Albelo, L. M.; Aznar Cervantes, S. D.; Lozano-Pérez, A. A.; Cenís, J. L.; Barea, E.; Navarro, J. A. *Angew. Chem., Int. Ed.* **2015**, *54*, 6790.

(8) Mondal, S. S.; Holdt, H. J. *Angew. Chem., Int. Ed.* **2016**, *55*, 42.

(9) Mondloch, J. E.; Katz, M. J.; Isley, W. C., III; Ghosh, P.; Liao, P.; Bury, W.; Wagner, G. W.; Hall, M. G.; DeCoste, J. B.; Peterson, G. W. *Nat. Mater.* **2015**, *14*, 512.

(10) Moon, S. Y.; Liu, Y.; Hupp, J. T.; Farha, O. K. *Angew. Chem., Int. Ed.* **2015**, *54*, 6795.

(11) Zhou, H.-C.; Long, J. R.; Yaghi, O. M. *Chem. Rev.* **2012**, *112*, 673.

(12) Getman, R. B.; Bae, Y.-S.; Wilmer, C. E.; Snurr, R. Q. *Chem. Rev.* **2012**, *112*, 703.

(13) Suh, M. P.; Park, H. J.; Prasad, T. K.; Lim, D.-W. *Chem. Rev.* **2012**, *112*, 782.

(14) Sumida, K.; Rogow, D. L.; Mason, J. A.; McDonald, T. M.; Bloch, E. D.; Herm, Z. R.; Bae, T.-H.; Long, J. R. *Chem. Rev.* **2012**, *112*, 724.

(15) Plonka, A. M.; Chen, X.; Wang, H.; Krishna, R.; Dong, X.; Banerjee, D.; Woerner, W. R.; Han, Y.; Li, J.; Parise, J. B. *Chem. Mater.* **2016**, *28*, 1636.

(16) Banerjee, D.; Simon, C. M.; Plonka, A. M.; Motkuri, R. K.; Liu, J.; Chen, X.; Smit, B.; Parise, J. B.; Haranczyk, M.; Thallapally, P. K. *Nat. Commun.* **2016**, *7*, 10.1038/ncomms11831.

(17) DeCoste, J. B.; Peterson, G. W. *Chem. Rev.* **2014**, *114*, 5695.

(18) Furukawa, H.; Cordova, K. E.; O'Keeffe, M.; Yaghi, O. M. *Science* **2013**, *341*, 1230444.

(19) Lee, J.; Farha, O. K.; Roberts, J.; Scheidt, K. A.; Nguyen, S. T.; Hupp, J. T. *Chem. Soc. Rev.* **2009**, *38*, 1450.

(20) Stassen, I.; Bueken, B.; Reinsch, H.; Oudenhoven, J.; Wouters, D.; Hajek, J.; Van Speybroeck, V.; Stock, N.; Vereecken, P.; Van Schaijk, R. *Chem. Sci.* **2016**, *7*, 5827−5832.

(21) Bai, Y.; Dou, Y.; Xie, L.-H.; Rutledge, W.; Li, J.-R.; Zhou, H.-C. *Chem. Soc. Rev.* **2016**, *45*, 2327.

(22) Mondloch, J. E.; Katz, M. J.; Planas, N.; Semrouni, D.; Gagliardi, L.; Hupp, J. T.; Farha, O. K. *Chem. Commun.* **2014**, *50*, 8944.

(23) Shearer, G. C.; Chavan, S. M.; Ethiraj, J.; Vitillo, J. G.; Svelle, S.; Olsbye, U.; Lamberti, C.; Bordiga, S.; Lillerud, K. P. *Chem. Mater.* **2014**, *26*, 4068−4071.

(24) Moon, S.-Y.; Wagner, G. W.; Mondloch, J. E.; Peterson, G. W.; DeCoste, J. B.; Hupp, J. T.; Farha, O. K. *Inorg. Chem.* **2015**, *54*, 10829.

(25) Peterson, G. W.; Moon, S.-Y.; Wagner, G. W.; Hall, M. G.; DeCoste, J. B.; Hupp, J. T.; Farha, O. K. *Inorg. Chem.* **2015**, *54*, 9684.

(26) Bordiga, S.; Bonino, F.; Lillerud, K. P.; Lamberti, C. *Chem. Soc. Rev.* **2010**, *39*, 4885.

(27) Singh, J.; Lamberti, C.; van Bokhoven, J. A. *Chem. Soc. Rev.* **2010**, *39*, 4754.

(28) Chavan, S.; Vitillo, J. G.; Gianolio, D.; Zavorotynska, O.; Civalleri, B.; Jakobsen, S.; Nilsen, M. H.; Valenzano, L.; Lamberti, C.; Lillerud, K. P. *Phys. Chem. Chem. Phys.* **2012**, *14*, 1614.

(29) Mondloch, J. E.; Bury, W.; Fairen-Jimenez, D.; Kwon, S.; DeMarco, E. J.; Weston, M. H.; Sarjeant, A. A.; Nguyen, S. T.; Stair, P. C.; Snurr, R. Q. *J. Am. Chem. Soc.* **2013**, *135*, 10294.

(30) Furukawa, H.; Gándara, F.; Zhang, Y.-B.; Jiang, J.; Queen, W. L.; Hudson, M. R.; Yaghi, O. M. *J. Am. Chem. Soc.* **2014**, *136*, 4369.

(31) Young, D. S. *The Rietveld method*; Oxford University Press: Oxford, U.K., 1993.

(32) Valenzano, L.; Civalleri, B.; Chavan, S.; Bordiga, S.; Nilsen, M. H.; Jakobsen, S.; Lillerud, K. P.; Lamberti, C. *Chem. Mater.* **2011**, *23*, 1700.

(33) Chapleski, R. C.; Musaev, D. G.; Hill, C. L.; Troya, D. *J. Phys. Chem. C* **2016**, *120*, 16822.

(34) Troya, D. *J. Phys. Chem. C* **2016**, *120*, 29312.

DOI: 10.1021/jacs.6b11373
J. Am. Chem. Soc. 2017, 139, 599−602